SCIENCE CHINA Materials ARTICLES

mater.scichina.com link.springer.com

Published online 21 September 2020 | https://doi.org/10.1007/s40843-020-1436-5
Sci China Mater 2020, 63(11): 2251–2260

SPECIAL TOPIC: Advanced Photocatalytic Materials

Surface modification of TiO_2 nanosheets with fullerene and zinc-phthalocyanine for enhanced photocatalytic reduction under solar-light irradiation

Liping Liu[1,2], Xiaolong Liu[1], Yongqiang Chai[1,2], Bo Wu[1*] and Chunru Wang[1*]

ABSTRACT **High-efficiency photocatalysts are of great importance to satisfy the requirements of green chemistry nowadays. Here we reported a novel solar-driven photocatalyst fabricated by a facile surface modification method, with the two-dimensional carboxylated zinc phthalocyanine-carboxylated C_{60}-titanium dioxide (ZnPc-C_3-TiO_2) nanosheets, in which the surface modifications of ZnPc and C_{60} derivative were designed to extend the absorption range and promote charge separation, respectively. Benefiting from the unique structure and positive synergetic effect, the ZnPc-C_3-TiO_2 nanocomposite shows promising applications in selective reduction of nitroarenes for high-value-added aromatic amines under solar light. Especially, for the photocatalytic reduction of nitrobenzene to aniline, the ZnPc-C_3-TiO_2 nanocomposite possesses both high efficiency and selectivity (up to 99%).**

Keywords: fullerene, TiO_2 nanosheet, electron-hole separation, photocatalytic activity

INTRODUCTION

Photocatalysis, which involves the absorption of light by one or more reacting species, is a green and sustainable technique to converse solar energy into chemical energy [1]. In recent years, scientific communities have focused intense interests on photocatalytic fuel generation, such as water splitting [2,3] and carbon dioxide reduction [4–7], yet the inadequacy in efficiency and endurance hampers their further application. Meanwhile, photocatalytic reduction techniques have shown great potential in fine chemical synthesis of high-value-added organic compounds [8,9]. For instance, the traditional catalytic hydrogenation, which usually adopts noble metal as the catalysts under harsh condition, is widely adopted for reducing nitrobenzene to aniline. However, with the development of photocatalysts, a more environment-friendly and low-cost approach to nitrobenzene reduction is anticipated [10].

Titanium dioxide (TiO_2) is a widely studied semiconductor material featuring high stability, easy preparation and low toxicity. Unfortunately, the photocatalytic performance of pristine TiO_2 is largely restricted by its broad bandgap (3.2 eV) and low quantum efficiency [11]. In fact, the construction of TiO_2-based nanocomposites, such as coupling with narrow band semiconductors or doping with non-metal/metal elements and loading with organic photosensitizer, has been proved to be effective strategies to boost the photocatalytic activity [12–15].

In the pursuit of highly efficient photocatalysts, the binary nanocomposites of TiO_2 modified with carbon nanomaterials, such as fullerene, carbon nanotube, and graphene, have drawn numerous attentions [16]. In particular, the C_{60}-modified TiO_2 nanocomposites have been reported to be able to efficiently catalyze the photodegradation of multiple organic substrates, such as Rhodamine B, methyl orange, and benzyl alcohol [17–19]. C_{60} is an excellent electron acceptor with high electron affinity and relatively small reorganization energy due to its rigid conjugate structure [20,21]. The incorporated C_{60} not only serves as a "reservoir" to accept the photogenerated electrons and thus inhibits unfavored charge recombination, but also broadens the light absorption range to a certain

[1] Beijing National Laboratory for Molecular Sciences, Key Laboratory of Molecular Nanostructure and Nanotechnology, Institute of Chemistry, Chinese Academy of Sciences, Beijing 100190, China
[2] School of Chemistry, University of Chinese Academy of Sciences, Beijing 100049, China
* Corresponding authors (emails: zkywubo@iccas.ac.cn (Wu B); crwang@iccas.ac.cn (Wang C))

degree [22–24]. However, the photocatalytic performance of the binary nanocomposites is still far from satisfactory due to the insufficient visible light utilization.

In order to optimize sunlight harvesting, numerous visible-light sensitizers have been proposed and widely adopted in dye-sensitized solar cells (DSSCs) [25,26]. Among those, phthalocyanines (Pcs) are known for their intrinsically intense absorption bands in both red/near-infrared (IR) (Q band) and ultraviolet (UV)/blue (Soret band) regions, extraordinary chemical and light stability, and suitable redox potential for the sensitization of large band-gap semiconductor [27–29]. Moreover, previous research suggests that the ZnPc sensitizer could satisfy efficient sensitization of TiO_2 photoanode *via* ultrafast electron ejection (~500 fs) from the excited state, making it one of the most promising candidates to promote solar light utilization [30].

Inspired by aforementioned insights, the ternary carboxylated zinc phthalocyanine-carboxylated C_{60}-titanium dioxide (ZnPc-C_3-TiO_2) nanosheet with excellent photocatalytic reduction activity was elaborately prepared. The two-dimensional TiO_2 nanosheets with a high specific surface area and abundant bonding sites were indispensable for additional surface modifications of carboxylated zinc phthalocyanine and C_{60}, which turned out to play a vital role in the improvement of catalytical performance. More specifically, the photogenerated electrons either from ZnPc under visible light excitation or from TiO_2 under UV light excitation would readily transfer to the electron-withdrawing C_{60} *via* energetically high-lying conduction band of TiO_2, leading to effective utilization of solar light and efficient separation of the photogenerated charge carriers. As a result, the well-designed ZnPc-C_3-TiO_2 composites display magnificent photocatalytic performance. The catalytic conversion efficiency for the reaction of nitrobenzene to aniline is more than 99%, and the selectivity of aniline is over 99%.

EXPERIMENTAL SECTION

Preparation of the C_3-TiO_2 nanosheets

The synthesis of carboxylated C_{60} ($C_{60}(C(COOH)_2)_3$, denoted as C_3) followed the same procedures described in Ref. [31]. Pure TiO_2 nanosheets (99 mg) [32] and 1 mg C_3 were then added into 50 mL ethanol and treated with ultrasonic for 30 min, followed by 15 min of stirring. The mixture was transferred to a 100-mL reactor and kept at 100°C for 12 h. After being cooled to room temperature, the precipitates were washed with ethanol and deionized water, and dried at 60°C for 12 h to obtain the C_3-TiO_2 nanosheets.

Preparation of the ZnPc-C_3-TiO_2 nanosheets

The zinc tetracarboxylic phthalocyanine (ZnPc) was prepared according to the previous work [33]. To the *N*,*N*-dimethylformamide (DMF) solution of ZnPc (10^{-4} mol L^{-1}), 100 mg C_3-TiO_2 nanosheets was added under continuous stirring. The crude samples were collected by centrifugation, followed by repeated rinsing with ethanol and distilled water. The samples were then dried at 80°C for 12 h to obtain the ZnPc-C_3-TiO_2 nanosheets.

Characterizations

The morphology and structure of the ZnPc-C_3-TiO_2 nanosheets were measured by scanning electron microscopy (SEM) (JSM-6700F JEOL, Japan), energy dispersive X-ray spectroscopy (EDS), transmission electron microscopy (TEM) and high-resolution TEM (HRTEM) (JEM-2100F, JEOL, Japan). *Ex-situ* atomic force microscopy (AFM, Bruker Corp., Dimension Icon) experiments were carried out in the Ar-filled glove box (Mikrouna, Super 1220/750, H_2O<0.1 ppm, O_2<0.1 ppm) by using an insulating silicon AFM tip (Bruker Corp., k=26 N m^{-1}, f_0=300 kHz), in the mode of PeakForce QNM (Quantitative Nano Mechanics). The phase structure was analyzed by X-ray diffraction (XRD, Bruker Corp.) with Cu Kα radiation source at 35 kV. The functional groups formed on the surface of the ternary nanosheets were examined by Fourier transform infrared (FT-IR) spectroscopy (Nicolet Inc., USA) using KBr pellets. Raman spectra were performed using a DXR Raman microscope (Thermo Scientific) equipped with a 532-nm laser as an excitation source at room temperature. The UV-Vis diffuse reflectance spectroscopy (DRS) measurements were carried out using a UV-Vis diffuse reflectance spectrophotometer (UV-3100, Shimadzu Inc., Japan) using $BaSO_4$ as the reflectance standard material. The chemical states of the elements in the sample were analyzed with an X-ray photoelectron spectroscopy (XPS, XSAM800, Kratos Analytical Inc., UK). Gas chromatography mass spectrometry (GCMS) analysis was performed on Shimadzu, GCMS-QP2010 Ultra Gas chromatograph mass spectrometer. The electron paramagnetic resonance (EPR) measurements were carried out on a JEOL JES-FA200 spectrometer. The photoelectrochemical measurements were conducted by an electrochemical workstation (CHI660E) using a conventional three-electrode system. A Pt wire and a saturated calomel electrode (SCE) were used as the counter and reference electrodes, respectively. For the working electrodes, the photocatalyst (3 mg) was dispersed in ethanol (0.5 mL) to obtain a slurry. Then the slurry (20 μL) was coated onto the FTO glass and dried in

an oven overnight. A 300 W Xe lamp with AM 1.5 G filter was used as the light source and the electrolyte was 0.5 mol L^{-1} Na_2SO_4 solution. The photocurrent response was recorded at a constant potential of 0.2 V. The electrochemical impedance spectroscopy (EIS) was carried out at an open-circuit voltage in a frequency range of 0.05–10^5 Hz with an amplitude of 5 mV.

Photocatalytic activity measurement

Photocatalytic reduction of nitroarenes to the corresponding aromatic amines was performed in a quartz vial. Firstly, 15 mg catalyst was fully dispersed in 2.25 mL H_2O/2-propanol (1:9) with 0.05 mmol nitroarenes and 0.4 mmol formic acid. Secondly, the above mixture was irradiated with a 300 W Xe arc lamp (CEL-HXUV300) with an AM 1.5 G filter to simulate solar irradiation, outputting the light density of 286 mW cm^{-2}. Thirdly, the suspension was centrifuged at 12,000 r min^{-1} for 3 min to remove the catalyst, and the remaining supernatant was analyzed by GC (Shimadzu GC-2014). The photocatalytic reaction was carried out under sealing condition after 20 mL min^{-1} N_2 bubbling for 30 min. Conversion of the nitroarene, yield of the aromatic amine and selectivity towards the aromatic amine were calculated [16] according to the following equations:

$$\text{Conversion } (\%) = [(C_0 - C_r) / C_0] \times 100,$$

$$\text{Yield } (\%) = (C_p / C_0) \times 100,$$

$$\text{Selectivity } (\%) = [C_p / (C_0 - C_r)] \times 100,$$

where C_0 is the initial concentration of the nitroarene, C_r and C_p are the concentrations of the resulting nitroarene and the targeted aromatic amine product at the end of the photocatalytic reaction.

RESULTS AND DISCUSSION

The ternary ZnPc-C_3-TiO_2 nanosheets were synthesized using a surface-modification method [29,34]. C_3 and ZnPc were immobilized on the surface of TiO_2 nanosheets in two steps, as shown in Scheme 1. The nanostructure of the as-prepared sample was characterized by TEM. As displayed in Fig. 1a, the ZnPc-C_3-TiO_2 nanosheets consisted of ultrathin sheet-like structures with an average thickness of about 4.2 nm, which is consistent with the AFM results (Fig. S1). Compared with the pristine TiO_2 nanosheets (Fig. S2), little change in the overall morphology was observed after two-step surface modification, indicating that the modification will not

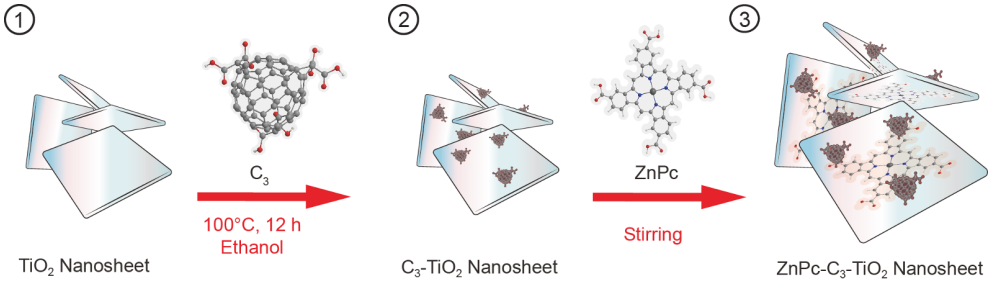

Scheme 1 Preparation of the ternary ZnPc-C_3-TiO_2 nanosheets.

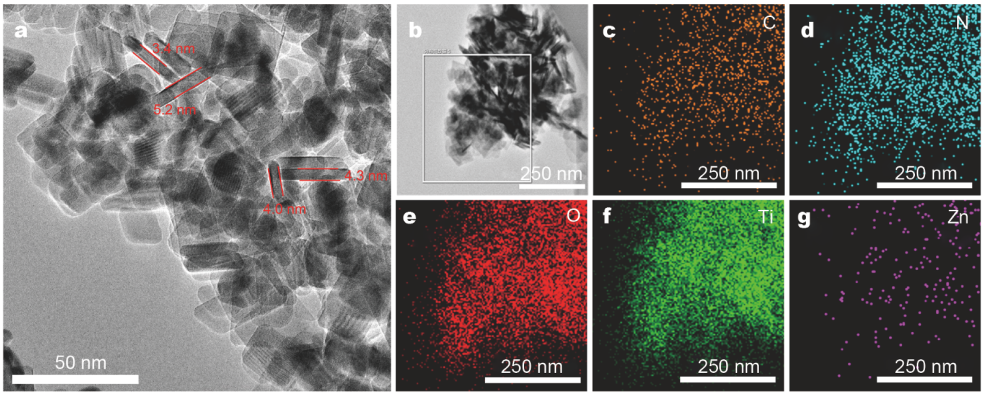

Figure 1 (a) TEM image and (b–g) EDS elemental mapping images of ZnPc-C_3-TiO_2 nanosheets.

undermine the sheet-like structure of the photocatalyst. The TEM-EDS elemental mapping images of the ZnPc-C_3-TiO_2 nanosheets are presented in Fig. 1b–g, which clearly display the uniformly distributed signals of Ti, C, O, Zn, and N. Moreover, the XRD pattern of the initial TiO_2 nanosheets was assigned to the typical structure of anatase phase in Fig. 2a [35,36]. After surface modification, the XRD pattern of ZnPc-C_3-TiO_2 nanosheets display almost the same characteristic peaks as that of the pristine TiO_2, indicating that the crystalline form of TiO_2 nanosheets remains virtually unchanged, coincident with the TEM results.

To further elucidate the chemical composition, FT-IR measurements were carried out. The spectrum of the pristine TiO_2 nanosheet features (Fig. 2b) with a broad band in the range of 400–1000 cm^{-1}, ascribed to the stretching vibration of Ti–O–Ti bonds (457 cm^{-1}) and Ti–O bonds (712 and 889 cm^{-1}). However, it should be noted that the band is evidently shifted in the C_3-TiO_2 hybrid, due to the significant interaction between TiO_2 and C_3 [37]. Further investigation of the interaction was performed based on the XPS and Raman experiments. As shown in Fig. S3, the high resolution XPS spectrum of C_3-TiO_2 hybrid shows two peaks assigned to Ti $2p_{3/2}$ and Ti $2p_{1/2}$, which shift to low binding energy compared with the pristine TiO_2, suggesting the non-ignorable bond interaction between C_3 and TiO_2 [38,39]. For the Raman spectrum of the C_3-TiO_2 composite (Fig. S4), besides the characteristic peaks of TiO_2 with $E_g(1)$, $B1_g(1)$, $A1_g(1)$ and $E_g(2)$ vibration [40], the fullerene-related Raman peaks were also observed in the range of 1200–1600 cm^{-1}, and correspondingly shifted compared with the original C_3, providing further evidence to the possible electron transfer from TiO_2 to C_3 [37]. In the case of ternary ZnPc-C_3-TiO_2 nanocomposites (Fig. 2b), the FT-IR spectrum shows discernible peaks at 1093, 1382, and 1527 cm^{-1}, which originated from the ZnPc (Fig. S5). It should be noted that the FT-IR spectrum of the ZnPc shows a broad band near 1700 cm^{-1}, ascribed to the asymmetric stretching vibration of carbonyl group in the carboxylic acid, which unexpectedly disappeared in the ternary composites [41]. This phenomenon is rationalized by considering that the ZnPc is chemically bonded to the TiO_2 surface *via* carboxylate groups, which play a crucial role in the efficient photogenerated charge injection from ZnPc to TiO_2 [42,43].

The light absorption property of the as-prepared photocatalyst was recorded in the diffuse reflectance spectra, as shown in Fig. 3. The pristine TiO_2 shows no absorption above its absorption edge at ca. 400 nm, meanwhile the C_3-TiO_2 hybrid only exhibits moderate absorption in the visible region. Once the light-harvesting ZnPc was further loaded, the light absorption of the ternary photocatalyst was significantly enhanced in the visible region, in favor of the utilization of solar light. From the UV-Vis DRS, the band gap energy of the as-prepared TiO_2 nanosheets can be calculated as 3.16 eV. Moreover, the flat-band potential of TiO_2 was determined to be −0.43 V *vs.* normal hydrogen electrode (NHE) (−0.63 V *vs.* Ag/AgCl) according to the Mott-Schottky plots (Fig. S6) [44]. In addition, the lowest unoccupied molecular orbital (LUMO) energy level of ZnPc was calculated to be −0.99 V *vs.* NHE (Table S1), indicating that the electron injection from the excited ZnPc into the conduction band of TiO_2 is thermodynamically feasible [45]. According to the DFT calculation, the highest occupied molecular orbital (HOMO) and HOMO-1 of the ZnPc are predominantly located on the internal macrocyclic structure, whereas the LUMO, LUMO-1 and LUMO-2 are partially delocalized over the

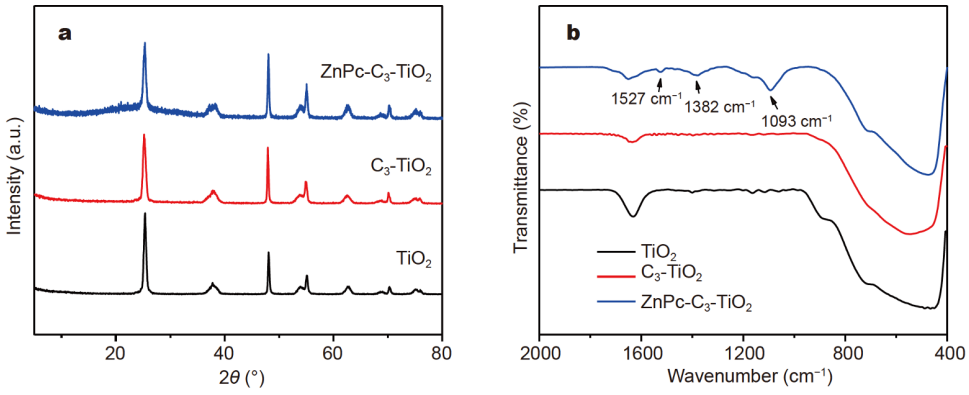

Figure 2 (a) XRD spectra and (b) FT-IR spectra of the pristine TiO_2, C_3-TiO_2 hybrid and ZnPc-C_3-TiO_2 nanosheets.

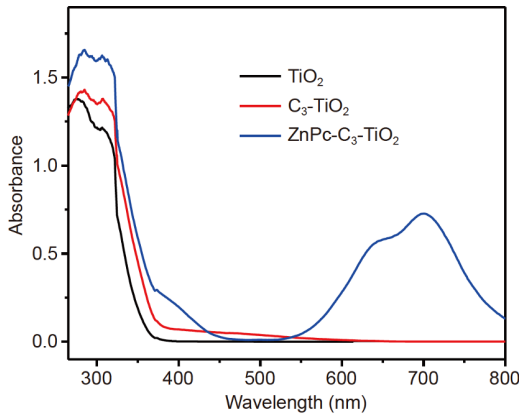

Figure 3 UV-Vis diffuse reflectance spectra of the pristine TiO_2, C_3-TiO_2 hybrid and ZnPc-C_3-TiO_2 nanosheets.

peripheral segment of the ZnPc, and further move to the carboxyl groups step by step (Fig. S7). The nature of the relevant frontier molecule orbitals suggests that the photoexcited electrons can transfer from the phthalocyanine skeleton to the carboxyl groups, which is beneficial to the electron injection of the excited ZnPc to TiO_2, and facilitates the visible-light-driven photoreduction activity eventually [46].

Photocatalytic activities

The photocatalytic reduction of nitrobenzene to aniline with the as-prepared photocatalysts was evaluated in the presence of formic acid as hole scavengers. As shown in Table 1, the ZnPc-C_3-TiO_2 photocatalyst affords superior performance for the nitrobenzene reduction reaction with high conversion rate (>99%) and selectivity (>99%) under simulated sunlight irradiation (Table 1, entry 5). In comparison, the conversion rate of nitrobenzene by the pristine TiO_2 is merely ca. 10% under the same conditions (Table 1, entry 1). After introduction of the C_{60} derivative, the conversion rates of C_3+TiO_2 (physical mixing) and C_3-TiO_2 (surface coating) nanosheets increase to 15.7% and 36.3% (Table 1, entries 2 and 3), respectively. The binary ZnPc-TiO_2 nanosheets also show a moderate conversion rate at ca. 35.5% (Table 1, entry 4), due to the improvement of light absorption [47]. Bearing the above results in mind, one can conclude that all the three components play an essential role in a synergetic manner to achieve high-efficiency photocatalysis.

In addition, the scope of nitroarene substrates was extended (Table 2). For the photocatalytic reductions of 4-, 3-, and 2-chloronitrobenzene, the reaction selectivity maintains as high as 99%. In the meantime, the corresponding conversion rates are 99%, 94% and 81%, respectively, at room temperature (Table 2, entries 1, 2 and 3), which shows a tendency of *p*-Cl > *m*-Cl > *o*-Cl, attributed to the steric effect around the NO_2 group [42]. Surprisingly, as a non-biodegradable pollutant, 4-nitrophenol molecules are proved to be reduced to 4-aminophenol using the ZnPc-C_3-TiO_2 photocatalyst (Table 2, entry 4) with high conversion rate (98%) and high selectivity (99%), and the reaction product is one of the potent intermediates for medicines, agrochemicals, and functional materials [48]. What is more, nitroarenes bearing either electron-donating or electron-withdrawing functional groups have been converted into corresponding aromatic amines with considerable conversion rates (entries 5 and 6), suggesting that the photocatalyst is of great potential for wide applications.

The stability of the photocatalyst is another important factor for practical use. This property was characterized by conducting five-run cycling experiments of photocatalytic nitrobenzene reduction under solar irradiation for 5 h. After that, the refreshed ZnPc-C_3-TiO_2 photocatalyst exhibits no remarkable decrease in both conversion rate and selectivity compared with the initial sample (Fig. S8). Further XRD (Fig. S9) and SEM (Fig. S10) characterizations also show no obvious change of the

Table 1 Reduction of nitrobenzene to aniline by different catalysts[a, b]

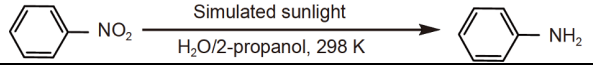

Entry	Catalyst	HCOOH (equiv)[c]	Conversion (%)	Selectivity (%)
1	TiO_2	8	10.3	98
2	C_3+TiO_2	8	15.7	96
3	C_3-TiO_2	8	36.3	99
4	ZnPc-TiO_2	8	35.5	96
5	ZnPc-C_3-TiO_2	8	99	99

a) Reaction conditions: nitrobenzene (0.050 mmol), photocatalyst (15 mg), H_2O/2-propanol (1:9, 2.25 mL), photoirradiation with a Xenon lamp through an AM 1.5 G filter, temperature=293 K, time=8 h. b) Determined by GC analysis; c) based on nitrobenzene.

Table 2 Reduction of nitroarenes to aromatic amines[a]

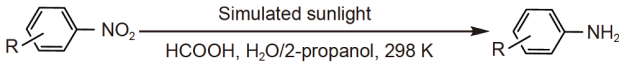

Entry	Substrate	Product	t (h)	Conversion (%)[b]	Selectivity (%)[c]
1	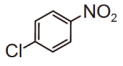	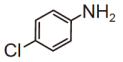	12	99	99
2	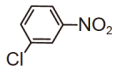	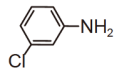	12	94	99
3	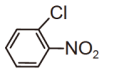	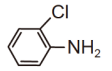	12	81	99
4	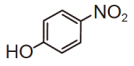	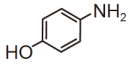	8	98	99
5	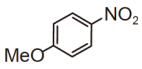	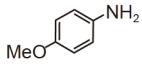	8	93	99
6	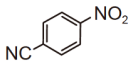	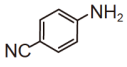	12	87	99

a) Reaction conditions: nitroarene (0.050 mmol), HCOOH (18.4 mg, 8.0 equiv based on nitroarenes), ZnPc-C_3-TiO_2 nanosheets (15 mg), H_2O/2-propanol (1:9, 2.25 mL), photoirradiation with a Xenon lamp through an AM 1.5 G filter, temperature=293 K. b) Determined by GC analysis; c) turn over frequency calculated based on the isolated yield of pure product.

sample after five cycles [49].

Mechanisms of photocatalytic activity

In order to clarify the detailed process of photogenerated charge carrier separation and recombination in the ZnPc-C_3-TiO_2 nanocomposite, photoluminescence (PL) measurement was systematically performed [50]. Upon UV excitation at 300 nm, the steady state PL spectra were severally recorded for TiO_2, C_3-TiO_2 and ZnPc-C_3-TiO_2 in the range of 320–420 nm (Fig. 4a), in which the prominent peak at ca. 375 nm is ascribed to the bandgap transition of TiO_2 [51]. Compared with the pristine TiO_2 and C_3-TiO_2, it is obvious that the PL emission of the ZnPc-C_3-TiO_2 nanocomposite is much weaker. There are two main reasons accounting for the PL quenching in the ternary photocatalyst. On one hand, the electron-withdrawing C_{60} component serves as an excellent acceptor for the photogenerated electron in the conduction band of TiO_2, and thus inhibits the charge carrier recombination process, which is also seen in the C_3-TiO_2 hybrid [37,52,53]. On the other hand, the ZnPc with moderate UV absorption ability is also supposed to exert a quenching effect, which would not contribute to the charge carrier separation [54]. In the current study, the former should be the major factor accounting for the superior photocatalytic activity in the ternary nanocomposite. Afterwards, the PL emission of ZnPc was investigated using visible excitation at 600 nm (Fig. S11). Similarly, significant quenching effect was observed in the ZnPc-C_3-TiO_2 photocatalyst, as a consequence of efficient electron transfer from the excited state of photosensitizer into the conduction band of TiO_2 [55,56].

To disclose the enhancing effect of C_{60} and ZnPc on the photocatalytic activity, the photoelectrochemical properties of the ZnPc-C_3-TiO_2 nanocomposite were systematically examined. The photocurrent transient responses were recorded for the photoelectrodes consisting of the pristine TiO_2, C_3-TiO_2 hybrid and ZnPc-C_3-TiO_2 composite, separately. As shown in Fig. 4b, the ternary ZnPc-C_3-TiO_2 composite exhibits substantially improved photocurrent compared with either the pristine TiO_2, or the C_3-TiO_2 hybrid. Benefiting from both the extended light absorption range and effective photogenerated charge separation due to the modifications of ZnPc and C_{60}, increased charge carriers have been generated and transferred under solar light irradiation [37]. The electron

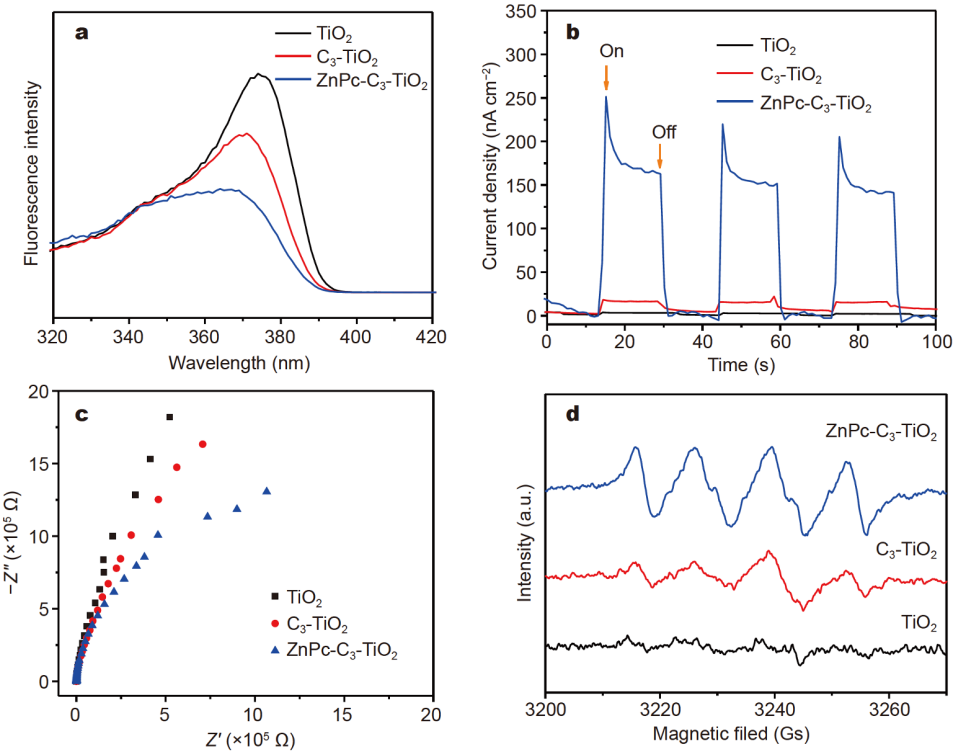

Figure 4 (a) PL emission spectra, (b) transient photocurrent responses, (c) EIS image and (d) EPR spectra of the TiO_2, C_3-TiO_2 and ZnPc-C_3-TiO_2 sample.

transport resistance of the ZnPc-C_3-TiO_2 photocatalyst was further measured by EIS, and the as-obtained Nyquist plots are depicted in Fig. 4c. Generally, each arc in the plot represents a resistance during the charge transfer process, and a smaller radius correlates to a lower charge-transfer resistance [57]. Accordingly, the radius of the ZnPc-C_3-TiO_2 composite is much smaller than that of the pure TiO_2 and C_3-TiO_2 hybrid, suggesting the lower charge transfer resistance and more effective charge separation in the ternary composite. These findings perfectly coincide with the results obtained from the photoresponse measurements [58].

For better interpretation of the photocatalytic reduction process, a simulation experiment was carried out utilizing EPR technique (Fig. 4d). In the presence of methanol as hole scavenger, the photogenerated free electron, readily captured by oxygen, gives rise to the formation and accumulation of superoxide radicals [59,60]. A widely used spin trap, 5,5-dimethyl-pyrroline *N*-oxide (DMPO), is applied to detect the active superoxide intermediates, which display four characteristic peaks in the EPR spectra [61]. As anticipated, the ZnPc-C_3-TiO_2 photocatalyst exhibits a more noticeable signal than those of the pristine TiO_2 or C_3-TiO_2 hybrid, in line with its outstanding photocatalytic performance. It is noticed that the strongly reductive $\cdot CO_2^-$ radicals, formed when the photogenerated holes are consumed by the formic acid scavenger, are also supposed to play a vital role in the photocatalytic reactions [62]. Correspondingly, a significant EPR signal ascribed to $\cdot CO_2^-$ radicals is revealed in the presence of formic acid as hole scavengers (Fig. S12).

According to the above results and discussions, a plausible mechanism of photocatalytic reduction of nitroarenes over the ZnPc-C_3-TiO_2 photocatalyst was proposed and illustrated in Fig. 5. Under solar-light irradiation, both TiO_2 nanosheets and ZnPc absorb photons, and then generate electron/hole pairs in the TiO_2 nanosheet and excited state ZnPc, respectively. Due to the chemically bonded interaction between the carboxylated derivatives and TiO_2 nanosheets, the photogenerated electrons either from ZnPc under visible light excitation or TiO_2 under UV light excitation would readily transfer to the electron-withdrawing C_{60} *via* the conduction band of TiO_2. As a result, successful spatial electron-hole separation occurs, leading to the suppression of the unfavorable photogenerated carrier recombination. Moreover, in the presence of hole

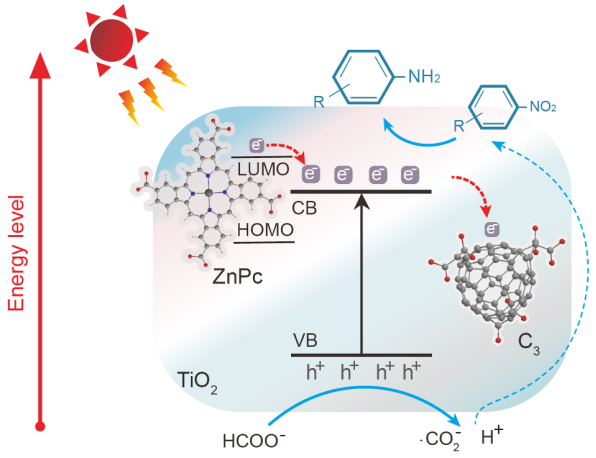

Figure 5 Mechanism of the photocatalytic reduction of nitrobenzene by ZnPc-C_3-TiO_2 under solar light irradiation.

scavengers and protons, the reductive free electrons and $\cdot CO_2^-$ radicals are capable of reducing the nitroarene substrates to aromatic amines on the surface of the ZnPc-C_3-TiO_2 nanosheets [63,64].

CONCLUSIONS

A novel ZnPc-C_3-TiO_2 nanocomposite was fabricated for the photocatalytic reduction of nitroarenes to high-value-added aromatic amines. Two-step surface modification was adopted in the modification of the pristine TiO_2 nanosheets with C_3 and ZnPc. Comprehensive morphology studies along with surface and interface analyses have shed light on the chemically bonded interactions between TiO_2 nanosheets and C_3/ZnPc, which play a vital role in the efficient charge separation. On one hand, the incorporated C_{60} serves as an excellent reservoir to accept the photogenerated electron from the conduction band of TiO_2, quenching the PL emission of the pristine TiO_2. On the other hand, the ZnPc significantly increases the light absorbing ability of the photocatalyst in the visible and near infrared region. Benefiting from the positive synergetic effect of the three components, the ZnPc-C_3-TiO_2 nanocomposite shows a promising photocatalytic performance in the reduction of the nitroarenes to the high-value-added aromatic amines, with a high selectivity and stability. These findings will broadly contribute to the development of novel photocatalysts in organic synthesis.

Received 19 May 2020; accepted 22 June 2020; published online 21 September 2020

1 Cheng L, Li X, Zhang H, *et al.* Two-dimensional transition metal MXene-based photocatalysts for solar fuel generation. J Phys Chem Lett, 2019, 10: 3488–3494
2 Zhao Z, Xing Y, Li H, *et al.* Constructing CdS/Cd/doped TiO_2 Z-scheme type visible light photocatalyst for H_2 production. Sci China Mater, 2018, 61: 851–860
3 Xu Q, Cheng B, Yu J, *et al.* Making co-condensed amorphous carbon/g-C_3N_4 composites with improved visible-light photocatalytic H_2-production performance using Pt as cocatalyst. Carbon, 2017, 118: 241–249
4 Cao S, Shen B, Tong T, *et al.* 2D/2D heterojunction of ultrathin MXene/Bi_2WO_6 nanosheets for improved photocatalytic CO_2 reduction. Adv Funct Mater, 2018, 28: 1800136
5 Richardson RD, Holland EJ, Carpenter BK. A renewable amine for photochemical reduction of CO_2. Nat Chem, 2011, 3: 301–303
6 Gao C, Meng Q, Zhao K, *et al.* Co_3O_4 hexagonal platelets with controllable facets enabling highly efficient visible-light photocatalytic reduction of CO_2. Adv Mater, 2016, 28: 6485–6490
7 Zhao K, Zhao S, Gao C, *et al.* Metallic cobalt-carbon composite as recyclable and robust magnetic photocatalyst for efficient CO_2 reduction. Small, 2018, 14: 1800762
8 Wu H, Mei S, Cao X, *et al.* Facile synthesis of Pt/Pd nanodendrites for the direct oxidation of methanol. Nanotechnology, 2014, 25: 195702
9 Liu L, Liu H, Zhao YP, *et al.* Directed synthesis of hierarchical nanostructured TiO_2 catalysts and their morphology-dependent photocatalysis for phenol degradation. Environ Sci Technol, 2008, 42: 2342–2348
10 Shiraishi Y, Togawa Y, Tsukamoto D, *et al.* Highly efficient and selective hydrogenation of nitroaromatics on photoactivated rutile titanium dioxide. ACS Catal, 2012, 2: 2475–2481
11 Fan Y, Hu G, Yu S, *et al.* Recent advances in TiO_2 nanoarrays/graphene for water treatment and energy conversion/storage. Sci China Mater, 2018, 62: 325–340
12 Liu X, Xing Z, Zhang Y, *et al.* Fabrication of 3D flower-like black N-TiO_{2-x}@MoS_2 for unprecedented-high visible-light-driven photocatalytic performance. Appl Catal B-Environ, 2017, 201: 119–127
13 Pan X, Yang MQ, Fu X, *et al.* Defective TiO_2 with oxygen vacancies: Synthesis, properties and photocatalytic applications. Nanoscale, 2013, 5: 3601–3614
14 Fang W, Xing M, Zhang J. A new approach to prepare Ti^{3+} self-doped TiO_2 *via* $NaBH_4$ reduction and hydrochloric acid treatment. Appl Catal B-Environ, 2014, 160-161: 240–246
15 Zhao K, Zhao S, Qi J, *et al.* Cu_2O clusters grown on TiO_2 nanoplates as efficient photocatalysts for hydrogen generation. Inorg Chem Front, 2016, 3: 488–493
16 Yang MQ, Zhang N, Xu YJ. Synthesis of fullerene-, carbon nanotube-, and graphene-TiO_2 nanocomposite photocatalysts for selective oxidation: A comparative study. ACS Appl Mater Interfaces, 2013, 5: 1156–1164
17 Wang S, Liu C, Dai K, *et al.* Fullerene C_{70}-TiO_2 hybrids with enhanced photocatalytic activity under visible light irradiation. J Mater Chem A, 2015, 3: 21090–21098
18 Meng ZD, Zhu L, Choi JG, *et al.* Effect of Pt treated fullerene/TiO_2 on the photocatalytic degradation of MO under visible light. J Mater Chem, 2011, 21: 7596–7603
19 Zhang L, Wang Y, Xu T, *et al.* Surface hybridization effect of C_{60} molecules on TiO_2 and enhancement of the photocatalytic activity. J Mol Catal A-Chem, 2010, 331: 7–14
20 Chai B, Liao X, Song F, *et al.* Fullerene modified C_3N_4 composites with enhanced photocatalytic activity under visible light irradiation. Dalton Trans, 2014, 43: 982–989
21 Meng ZD, Peng MM, Zhu L, *et al.* Fullerene modification CdS/

TiO_2 to enhancement surface area and modification of photocatalytic activity under visible light. Appl Catal B-Environ, 2012, 113-114: 141–149
22 Bilal Tahir M, Nabi G, Rafique M, *et al.* Role of fullerene to improve the WO_3 performance for photocatalytic applications and hydrogen evolution. Int J Energy Res, 2018, 42: 4783–4789
23 Meng ZD, Zhu L, Choi JG, *et al.* Preparation, characterization and photocatalytic behavior of WO_3-fullerene/TiO_2 catalysts under visible light. Nanoscale Res Lett, 2011, 6: 459
24 Meng ZD, Ghosh T, Zhu L, *et al.* Synthesis of fullerene modified with Ag_2S with high photocatalytic activity under visible light. J Mater Chem, 2012, 22: 16127–16135
25 Lee SHA, Abrams NM, Hoertz PG, *et al.* Coupling of titania inverse opals to nanocrystalline titania layers in dye-sensitized solar cells. J Phys Chem B, 2008, 112: 14415–14421
26 Wu J, Hao S, Lin J, *et al.* Crystal morphology of anatase titania nanocrystals used in dye-sensitized solar cells. Cryst Growth Des, 2008, 8: 247–252
27 Wan Y, Cong T, Liang Q, *et al.* Facile *in-situ* solvothermal method to synthesize ZnPc-MWCNTs composites with enhanced visible light photocatalytic activity. Ceramics Int, 2016, 42: 2425–2430
28 Zhang M, Shao C, Guo Z, *et al.* Hierarchical nanostructures of copper(II) phthalocyanine on electrospun TiO_2 nanofibers: Controllable solvothermal-fabrication and enhanced visible photocatalytic properties. ACS Appl Mater Interfaces, 2011, 3: 369–377
29 Reddy P, Giribabu L, Lyness C, *et al.* Efficient sensitization of nanocrystalline TiO_2 films by a near-IR-absorbing unsymmetrical zinc phthalocyanine. Angew Chem, 2007, 119: 377–380
30 He J, Benkö G, Korodi F, *et al.* Modified phthalocyanines for efficient near-IR sensitization of nanostructured TiO_2 electrode. J Am Chem Soc, 2002, 124: 4922–4932
31 Lamparth I, Hirsch A. Water-soluble malonic acid derivatives of C_{60} with a defined three-dimensional structure. J Chem Soc Chem Commun, 1994, 14: 1727–1728
32 Han X, Kuang Q, Jin M, *et al.* Synthesis of titania nanosheets with a high percentage of exposed (001) facets and related photocatalytic properties. J Am Chem Soc, 2009, 131: 3152–3153
33 Bai M, Song R, Zhang Y, *et al.* Trimellitic anhydride- and pyromellitic dianhydride-originated tetrakis/octakis(octyloxycarbonyl) phthalocyaninato metal complexes. InOrg Chem Commun, 2013, 28: 99–103
34 Grinter DC, Woolcot T, Pang CL, *et al.* Ordered carboxylates on TiO_2 (110) formed at aqueous interfaces. J Phys Chem Lett, 2014, 5: 4265–4269
35 Yang K, Chen X, Zheng Z, *et al.* Solvent-induced surface disorder and doping-induced lattice distortion in anatase TiO_2 nanocrystals for enhanced photoreversible color switching. J Mater Chem A, 2019, 7: 3863–3873
36 Liu W, Liu Z, Wang G, *et al.* Carbon coated Au/TiO_2 mesoporous microspheres: A novel selective photocatalyst. Sci China Mater, 2017, 60: 438–448
37 Yu J, Ma T, Liu G, *et al.* Enhanced photocatalytic activity of bimodal mesoporous titania powders by C_{60} modification. Dalton Trans, 2011, 40: 6635–6644
38 Li B, Zhao Z, Gao F, *et al.* Mesoporous microspheres composed of carbon-coated TiO_2 nanocrystals with exposed {001} facets for improved visible light photocatalytic activity. Appl Catal B-Environ, 2014, 147: 958–964
39 Zhang P, Shao C, Zhang Z, *et al.* TiO_2@carbon core/shell nanofibers: controllable preparation and enhanced visible photocatalytic properties. Nanoscale, 2011, 3: 2943–2949
40 Lin J, Zong R, Zhou M, *et al.* Photoelectric catalytic degradation of methylene blue by C_{60}-modified TiO_2 nanotube array. Appl Catal B-Environ, 2009, 89: 425–431
41 Max JJ, Chapados C. Infrared spectroscopy of aqueous carboxylic acids: Comparison between different acids and their salts. J Phys Chem A, 2004, 108: 3324–3337
42 Qian W, Wei W, Hong M, *et al.* Microwave assisted synthesis of ZnPc-COOH and SiO_2/ZnPc-COOH nanopaticles: Singlet oxygen production and photocatalytic property. Colloids Surfs A-Physicochem Eng Aspects, 2014, 443: 52–59
43 Xu H. Synthesis of novel amphiphilic zinc phthalocyanines and fabrication of zinc phthalocyanine-titanium oxide multilayers. Dyes Pigments, 2001, 49: 9–14
44 Hamandi M, Berhault G, Guillard C, *et al.* Reduced graphene oxide/TiO_2 nanotube composites for formic acid photodegradation. Appl Catal B-Environ, 2017, 209: 203–213
45 Zhang X, Yu L, Li R, *et al.* Asymmetry and electronic directionality: A means of improving the red/near-IR-light-responsive photoactivity of phthalocyanine-sensitized carbon nitride. Catal Sci Technol, 2014, 4: 3251
46 Li K, Lin L, Peng T, *et al.* Asymmetric zinc porphyrin-sensitized nanosized TiO_2 for efficient visible-light-driven CO_2 photoreduction to CO/CH_4. Chem Commun, 2015, 51: 12443–12446
47 Huang Z, Zheng B, Zhu S, *et al.* Photocatalytic activity of phthalocyanine-sensitized TiO_2-SiO_2 microparticles irradiated by visible light. Mater Sci Semicond Process, 2014, 25: 148–152
48 Verho O, Nagendiran A, Tai CW, *et al.* Nanopalladium on amino-functionalized mesocellular foam as an efficient and recyclable catalyst for the selective transfer hydrogenation of nitroarenes to anilines. ChemCatChem, 2014, 6: 205–211
49 Nazeeruddin MK, Humphry-baker R, Grätzel M, *et al.* Efficient near-IR sensitization of nanocrystalline TiO_2 films by zinc and aluminum phthalocyanines. J Porphyrins Phthalocyanines, 2012, 03: 230–237
50 Hernández-Gordillo A, Romero AG, Tzompantzi F, *et al.* Kinetic study of the 4-nitrophenol photooxidation and photoreduction reactions using CdS. Appl Catal B-Environ, 2014, 144: 507–513
51 Wang E, Yang W, Cao Y. Unique surface chemical species on indium doped TiO_2 and their effect on the visible light photocatalytic activity. J Phys Chem C, 2009, 113: 20912–20917
52 Long Y, Lu Y, Huang Y, *et al.* Effect of C_{60} on the photocatalytic activity of TiO_2 nanorods. J Phys Chem C, 2009, 113: 13899–13905
53 Cho EC, Ciou JH, Zheng JH, *et al.* Fullerene C_{70} decorated TiO_2 nanowires for visible-light-responsive photocatalyst. Appl Surf Sci, 2015, 355: 536–546
54 Pompa PP, Ciccarella G, Spadavecchia J, *et al.* Spectroscopic investigation of inner filter effects by phthalocyanine solutions. J Photochem Photobiol A-Chem, 2004, 163: 113–120
55 Giribabu L, Vijay Kumar C, Gopal Reddy V, *et al.* Unsymmetrical alkoxy zinc phthalocyanine for sensitization of nanocrystalline TiO_2 films. Sol Energy Mater Sol Cells, 2007, 91: 1611–1617
56 Kc CB, Stranius K, D'Souza P, *et al.* Sequential photoinduced energy and electron transfer directed improved performance of the supramolecular solar cell of a zinc porphyrin-zinc phthalocyanine conjugate modified TiO_2 surface. J Phys Chem C, 2013, 117: 763–773
57 Zhang L, He X, Xu X, *et al.* Highly active TiO_2/g-C_3N_4/G photocatalyst with extended spectral response towards selective reduction of nitrobenzene. Appl Catal B-Environ, 2017, 203: 1–8

58 Hou JH, Lan X, Shi J, *et al.* A mild and simple method to fabricate commercial TiO_2 (P25) and C_{60} composite for highly enhancing H_2 generation. Int J Hydrogen Energy, 2020, 45: 2852–2861
59 Li Q, Hou X, Fang Z, *et al.* Construction of layered h-BN/TiO_2 hetero-structure and probing of the synergetic photocatalytic effect. Sci China Mater, 2019, 63: 276–287
60 Yu Z, Chen Z, Chen Y, *et al.* Photocatalytic hydrogenation of nitroarenes using $Cu_{1.94}S$-$Zn_{0.23}Cd_{0.77}S$ heteronanorods. Nano Res, 2018, 11: 3730–3738
61 Zhang Y, Tang ZR, Fu X, *et al.* TiO_2-graphene nanocomposites for gas-phase photocatalytic degradation of volatile aromatic pollutant: Is TiO_2-graphene truly different from other TiO_2-carbon composite materials? ACS Nano, 2010, 4: 7303–7314
62 Song Y, Wang H, Wang Z, *et al.* Selective photocatalytic synthesis of haloanilines from halonitrobenzenes over multifunctional AuPt/monolayer titanate nanosheet. ACS Catal, 2018, 8: 9656–9664
63 Fukui M, Koshida W, Tanaka A, *et al.* Photocatalytic hydrogenation of nitrobenzenes to anilines over noble metal-free TiO_2 utilizing methylamine as a hydrogen donor. Appl Catal B-Environ, 2020, 268: 118446
64 Ji Y, Fan T, Luo Y. First-principles study on the mechanism of photocatalytic reduction of nitrobenzene on the rutile TiO_2 (110) surface. Phys Chem Chem Phys, 2020, 22: 1187–1193

Acknowledgements This work was supported by Beijing Natural Science Foundation (2182094), and the National Natural Science Foundation of China (51772300 and 51832008). Wu B particularly thanks the Youth Innovation Promotion Association of CAS (2018039). We also thank Jianlei Tian for assistance in synthesis, and Jing Wan for assistance in AFM measurement.

Author contributions Liu L, Wu B and Wang C designed and engineered the experiments; Wang C and Wu B provided insights on the experiments and supervised the research; Liu L synthesized and characterized the samples; Liu X contributed to the theoretical analysis; Liu L, Chai Y and Liu X participated in the data analysis; Liu L wrote the paper with support from Wang C and Wu B. All authors contributed to the general discussion.

Conflict of interest The authors declare that they have no conflict of interest.

Supplementary information Supporting data are available in the online version of the paper.

Liping Liu is currently a PhD candidate at the Institute of Chemistry, Chinese Academy of Sciences. She received her MSc degree from the University of Science and Technology Beijing in 2017. Her PhD research focuses on the synthesis and design of fullerene-relevant nanomaterials and their applications in photocatalysis.

Bo Wu received her PhD degree from the Institute of Chemistry, Chinese Academy of Sciences in 2016. She worked as an assistant researcher at the Institute of Chemistry, Chinese Academy of Sciences from 2016 to 2019. She is now an associate professor at Beijing National Laboratory for Molecular Sciences, Key Laboratory of Molecular Nanostructure and Nanotechnology. Her research focuses on the photoelectric properties of fullerene-based nanocomposites.

Chunru Wang received his PhD degree in physical chemistry in 1992 from the Chinese Academy of Sciences. Currently, he is a professor in the Institute of Chemistry, Chinese Academy of Sciences. His research interests include the synthesis, isolation, and characterization of endohedral fullerenes and the industrial applications of fullerenes and metallofullerenes.

富勒烯和酞菁锌修饰的二氧化钛纳米片应用于太阳光下的光催化还原

刘丽萍[1,2], 刘晓龙[1], 柴永强[1,2], 吴波[1*], 王春儒[1*]

摘要 高效的光催化剂对于满足当今绿色化学的发展具有特别重要的意义. 本文采用表面修饰法, 制备了一种二维羧基锌酞菁-羧基C_{60}-二氧化钛(ZnPc-C_3-TiO_2)纳米片, 其中表面修饰的ZnPc和C_{60}衍生物分别用于扩展太阳光的吸收范围和促进光生电荷分离. 得益于其独特的结构和良好的协同效应, ZnPc-C_3-TiO_2纳米复合材料在太阳光下选择性光催化芳香硝基化合物还原为芳香胺的反应中显示出良好的应用前景. 特别地, 对于光催化硝基苯还原为苯胺的反应, ZnPc-C_3-TiO_2复合材料同时表现出较高的催化转化效率和选择性(均高达99%).

